# Effect of Rotor Cant on Trim and Autonomous Flight Dynamics of a Quadcopter

**Robert Niemiec**
Ph. D Candidate

**Farhan Gandhi**
Redfern Chair of Aerospace Engineering

Center for Mobility with Vertical Lift (MOVE)
Rensselaer Polytechnic Institute
Troy, NY, United States

## ABSTRACT

Rotor cant is simulated on an SUI Endurance quadcopter. Two types of rotor cant, flapwise and torsional cant, are defined, and multirotor coordinates are used to define four aircraft-level modes of cant for each type. Collective flapwise cant causes an increase in collective control and power required, and a positive correlation exists between collective flapwise cant and pitch control. It also causes the longitudinal and lateral poles to retreat from the origin. Postive longitudinal flapwise and negative lateral torsional cant cause a reduction in nose-down attitude in forward flight, reducing drag and negative lift on the fuselage by 13% and 31% at 15 m/s, which reduces power required by 6% while increasing hover power by only 0.5%. Lateral flapwise cant and longitudinal torsional cant affect the roll attitude, though no power savings is available. Differential flapwise cant causes forward speed to impose a net rolling moment, which is compensated by roll control. Differential torsional cant is positively correlated with roll control. Both differential cant modes cause some poles to move toward the origin while others move away, but differential torsional cant can increase yaw authority by up to 325%.

## INTRODUCTION

Electric VTOL-capable aircraft are flourishing in the field of vertical lift. Their mechanical simplicity makes them easy to build and operate, resulting in unprecedented accessibility and flexibility in their application. Multicopters, in particular, are finding uses from photography and surveillance to remote structural inspection. eVTOL platforms are also being explored for use as package delivery systems and as short-range passenger aircraft (Ref. 1).

Most eVTOL aircraft are driven by a distributed electric propulsion system. The array of rotors are individually speed-controlled to regulate their individual thrusts, which are used to control aircraft-level forces and moments, as opposed to conventional helicopters which use collective and cyclic pitch control on a single rotor to regulate forces and moments. The most common configuration of eVTOL aircraft is the multicopter, which typically has rotors arranged in a regular polygon, with adjacent rotors spinning in opposite directions. In most configurations, the rotor hubs are coplanar, and all thrusting in the same direction.

Built-in rotor cant is a common feature of large helicopters. For example, the UH-60 Blackhawk has a 3 degree forward tilt in its main rotor shaft to reduce rotor flapping in forward flight (Ref. 2), and its tail rotor is canted upward so it can contribute to aircraft thrust. Since electric vehicles do not require gearboxes to deliver power to the rotors, they have a great deal of flexibility in the orientations of their rotors. For example, Brescanini and D'Andrea built a cube-shaped octocopter, dubbed the "Omnicopter" (Ref. 3) that is controllable regardless of its orientation. Phillips et al. also employed rotor cant on a quadrotor biplane tailsitter to improve roll authority in its airplane configuration (Ref. 4).

**Fig. 1. Straight-Up Imaging Endurance**

## PLATFORM DESCRIPTION AND CANT DEFINITION

The present study explores the effect of general rotor cant on a quadcopter, as well as define types and modes of rotor cant on a general multicopter. The platform chosen is based on the Straight-Up Imaging (SUI) Endurance quadcopter (Ref. 5), shown in Fig. 1. This 3.2kg gross weight quadcopter has four, 15-inch rotors arranged in a cross-configuration. In Ref. 6, Russell and Sekula characterized the 2D aerodynamic properties of various sections of the SUI Endurance rotor through

Presented at the AHS International 74th Annual Forum & Technology Display, Phoenix, Arizona, USA, May 14–17, 2018.

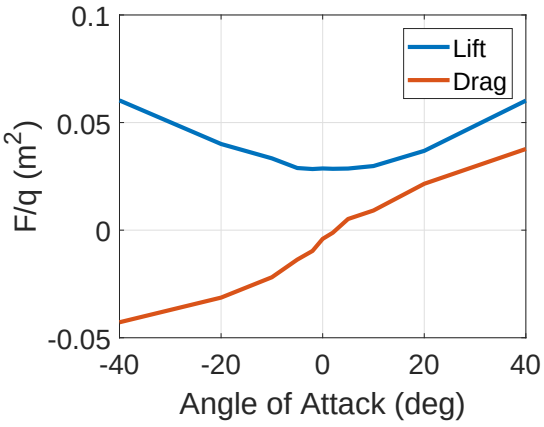


**Fig. 2. Aerodynamic loads on the fuselage, normalized by dynamic pressure, versus angle of attack (positive nose-up)**

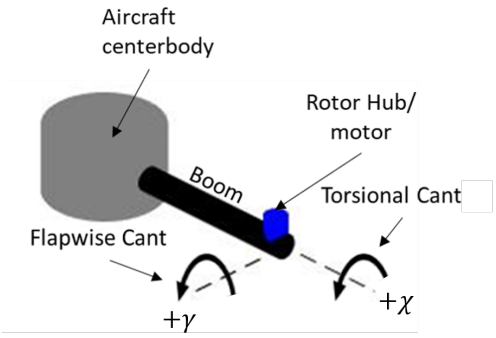


**Fig. 3. Cant Types**

CFD on a laser-scan of the rotor. Fuselage forces, normalized by dynamic pressure, are plotted in Fig. 2. This data was taken from wind-tunnel experiments on the bare airframe of the SUI Endurance by Russell et al. in Ref 7.

Beginning from this platform, the rotors are canted about two axes (Fig. 3), one extending radially from the geometric center of the aircraft, representing a torsional cant ($\chi$), and an axis orthogonal to that and the rotational axis of the uncanted rotor. Rotation about this axis is denoted as "flapwise cant" ($\gamma$). The sign convention used in this study has positive $\gamma$ resulting in the thrust pointing toward the aircraft centerbody, while positive $\chi$ results in the thrust vector undergoing a counter-clockwise rotation as viewed down the boom axis toward the centerbody.

Instead of defining the cant angles for each rotor individually, multi-rotor coordinates will be used to define modes at the aircraft level. Multi-rotor coordinates have previously been defined by the authors in their study of power-optimal controls of a multicopter (Ref. 8). The four modes of flapwise cant are illustrated in Fig. 4, and the redirection of thrust, as viewed from the top of the aircraft is illustrated in Fig. 5. Positive collective flapwise cant ($\gamma_0$, Fig. 4(a)) applies positive $\gamma$ to all rotors, vectoring thrust inboard (Fig. 5(a)), with no net forces except a decrease in vertical thrust. Lateral flapwise cant ($\gamma_{1s}$, Fig. 4(b)) cants rotors on the right side of the aircraft positively, and rotors on the left side negatively, reorienting overall thrust leftward (Fig. 5(b)). Positive longitudinal flapwise cant ($\gamma_{1c}$, Fig. 4(c)) cants rear rotors positively and front rotors negatively, reorienting thrust forward (Fig. 5(c)). Finally, differential flapwise cant ($\gamma_d$, Fig. 4(d)) alternates between negative and positive cant, starting with the front-right rotor. This results in counter-clockwise-spinning rotors (pictured in blue in Fig. 4) having negative cant, and clockwise-spinning rotors (pictured in red in Fig. 4) having positive cant. Thrust is redirected as shown in Fig. 5(d), and like collective flapwise cant, results no net forces, except a reduction in vertical thrust.

The four modes of torsional cant are plotted in Fig. 6. Collective torsional cant ($\chi_0$, Fig. 6(a), applies equally to all four rotors. This causes all four rotors' thrusts to produce a large nose-right moment about the aircraft C.G. (Fig. 7(a)), which the rotor torque is usually unable to compensate, meaning no trim solutions exist. Therefore, this cant mode is not used in this study. Lateral torsional cant ($\chi_{1s}$, Fig. 6(b) applies positive $\chi$ to rotors on the right, and negative $\chi$ to rotors on the left, resulting in a net aftward vectoring of thrust. Longtitudinal torsional cant ($\chi_{1c}$, Fig. 6(c) produces a net leftward thrust by canting forward rotors negatively and rear rotors positively. Differential torsional cant ($\chi_d$, Fig. 6(d)) alternates positive and negative torsional cant, so that counter-clockwise-spinning rotors are canted negatively, while clockwise-spinning rotors are canted positively. If the azimuthal angle, $\Psi$, is defined as zero at the aft of the aircraft and increasing counter-clockwise (as in Fig. 8), then a transformation from multi-rotor coordinates to individual-rotor coordinates is defined by Eq. 1, which can be used to determine the individual cant angles from the aircraft-level modes.

$$\begin{bmatrix}\gamma_1\\ \gamma_2\\ \gamma_3\\ \gamma_4\end{bmatrix} = \begin{bmatrix}1 & \sin\frac{3\pi}{4} & \cos\frac{3\pi}{4} & -1\\ 1 & \sin\frac{5\pi}{4} & \cos\frac{5\pi}{4} & 1\\ 1 & \sin\frac{7\pi}{4} & \cos\frac{7\pi}{4} & -1\\ 1 & \sin\frac{\pi}{4} & \cos\frac{\pi}{4} & 1\end{bmatrix}\begin{bmatrix}\gamma_0\\ \gamma_{1s}\\ \gamma_{1c}\\ \gamma_d\end{bmatrix} = \begin{bmatrix}1 & \frac{\sqrt{2}}{2} & -\frac{\sqrt{2}}{2} & -1\\ 1 & -\frac{\sqrt{2}}{2} & -\frac{\sqrt{2}}{2} & 1\\ 1 & -\frac{\sqrt{2}}{2} & \frac{\sqrt{2}}{2} & -1\\ 1 & \frac{\sqrt{2}}{2} & \frac{\sqrt{2}}{2} & 1\end{bmatrix}\begin{bmatrix}\gamma_0\\ \gamma_{1s}\\ \gamma_{1c}\\ \gamma_d\end{bmatrix} \quad (1)$$

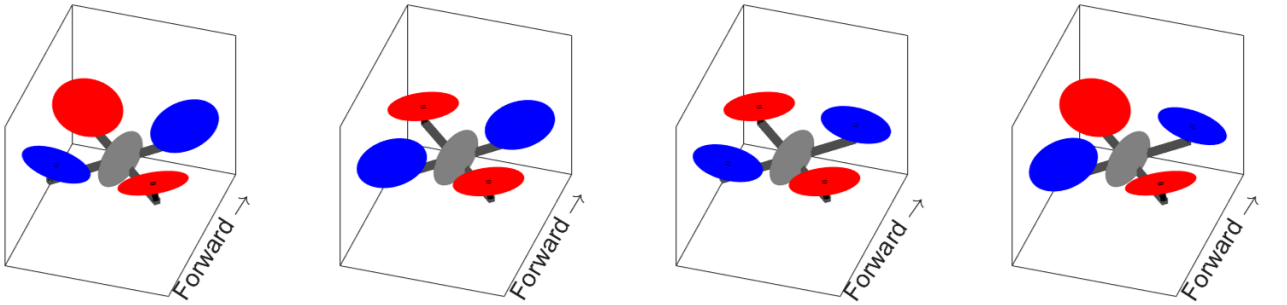


(a) Collective Flapwise Cant ($\gamma_0$) (b) Lateral Flapwise Cant ($\gamma_{1s}$) (c) Longidutinal Flapwise Cant ($\gamma_{1c}$) (d) Differential Flapwise Cant ($\gamma_d$)

**Fig. 4. Four modes of flapwise cant for a quadcopter**

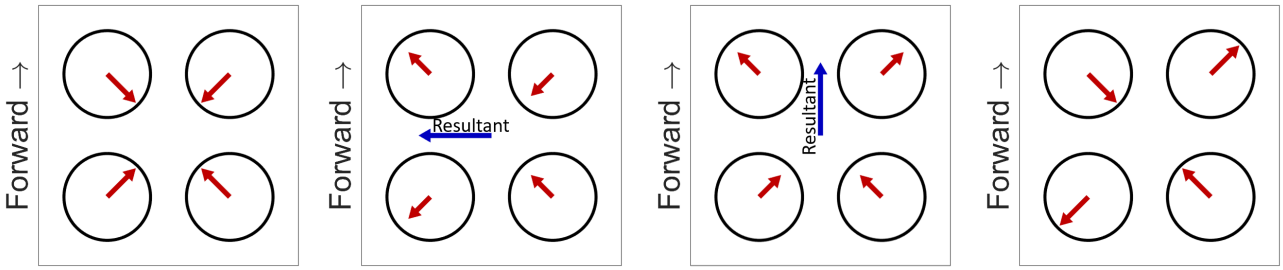


(a) Collective Flapwise Cant ($\gamma_0$) (b) Lateral Flapwise Cant ($\gamma_{1s}$) (c) Longidutinal Flapwise Cant ($\gamma_{1c}$) (d) Differential Flapwise Cant ($\gamma_d$)

**Fig. 5. In-plane component of thrust with each mode of flapwise cant (Resultant in blue)**

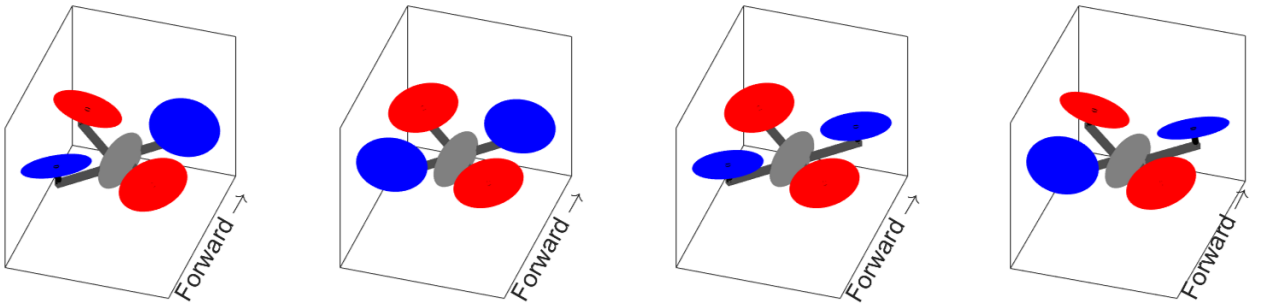


(a) Collective Torsional Cant ($\chi_0$) (b) Lateral Torsional Cant ($\chi_{1s}$) (c) Longidutinal Torsional Cant ($\chi_{1c}$) (d) Differential Torsional Cant ($\chi_d$)

**Fig. 6. Four modes of torsional cant for a quadcopter**

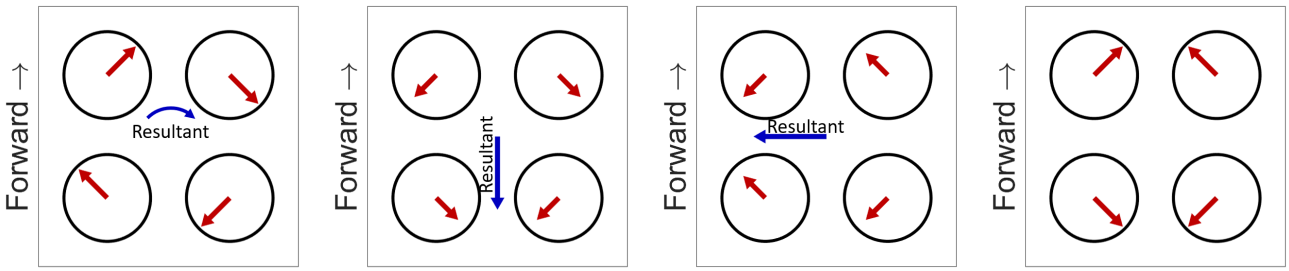


(a) Collective Torsional Cant ($\chi_0$) (b) Lateral Torsional Cant ($\chi_{1s}$) (c) Longidutinal Torsional Cant ($\chi_{1c}$) (d) Differential Torsional Cant ($\chi_d$)

**Fig. 7. In-plane component of thrust with each mode of torsional cant (Resultant in blue)**

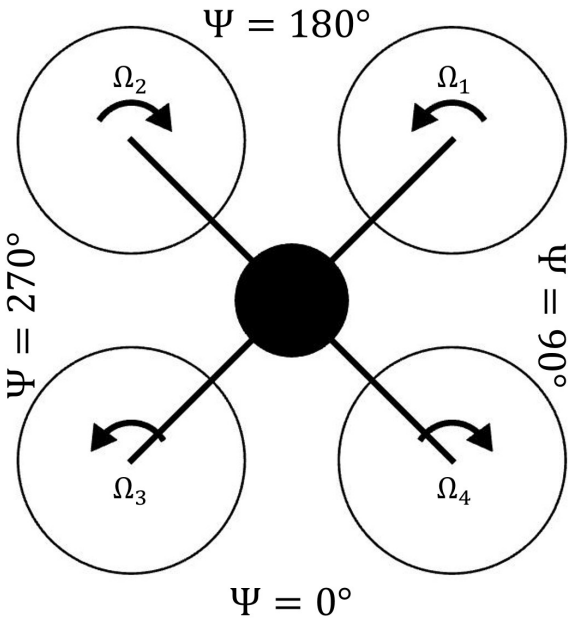


**Fig. 8. Top view of quadrotor**

As a fixed-pitch, variable RPM vehicle, the quadcopter is controlled by regulating the speed of the individual rotors. Often, these speeds are expressed in individual rotor coordinates. In this study, the controls are represented in multi-rotor coordinates, as in (Ref. 8). The multirotor controls of a quadcopter are illustrated in Fig. 9. The collective mode ($\Omega_0$, Fig. 9(a)) represents the average speed of the four rotors; changing its value increases or decreases the speed of all four rotors simultaneously. On a cant-free quadcopter in hover, this regulates vertical thrust without generating any other forces or moments. Roll control is given by applying a differential RPM between the left and right rotors ($\Omega_R$, Fig. 9(b)). Similarly, pitch and yaw control are provided by applying a differential RPM between the front/aft rotors ($\Omega_P$, Fig. 9(c)) and the counter-clockwise- and clockwise-spinning rotors ($\Omega_Y$, Fig. 9(d)). Individual rotor speeds can be determined through a coordinate transformation identical to Eq. 1.

## MODELING

To assess the effect of rotor cant on aerodynamic performance, a dynamic simulation is implemented. Accelerations on the aircraft are calcualted via sum of forces and moments about the aircraft center of gravity, assumed to lie below the rotor plane at the geometric center of the aircraft. The forces include gravity, rotor loads, and fuselage drag. Rotor forces and moments are calculated via blade element theory, using a 10-state Peters-He finite-state dynamic wake model on each rotor. It was previously shown that this number of states captures the average forces and moments of a multicopter rotor at this scale ( (Ref. 9)). Rotor-rotor and rotor-fuselage interference is neglected in this study.

Vectors in this study are defined with respect to one of several reference frames. The first is an inertial reference frame, attached to an arbitrary fixed point in space. The axes are defined with a North-East-Down convention. The second reference frame is a body-attached frame, also with a North-East-Down convention, with North and East being defined as $\Psi = 180^\circ$ and $\Psi = 90^\circ$ as shown in Fig. 8, respectively. Rotation from the inertial to the body reference frame is defined using a 3-2-1 Euler rotation (Eq. 2, where $c_\square = \cos(\square)$, $s_\square = \sin(\square)$), while $\phi$, $\theta$, and $\psi$ are the roll, pitch, and yaw attitudes, respectively.

$$\begin{aligned} R_{b/i} &= R_\phi R_\theta R_\psi \\ &= \begin{bmatrix} 1 & 0 & 0 \\ 0 & c_\phi & s_\phi \\ 0 & -s_\phi & c_\phi \end{bmatrix} \begin{bmatrix} c_\theta & 0 & -s_\theta \\ 0 & 1 & 0 \\ s_\theta & 0 & c_\theta \end{bmatrix} \begin{bmatrix} c_\psi & s_\psi & 0 \\ -s_\psi & c_\psi & 0 \\ 0 & 0 & 1 \end{bmatrix} \\ &= \begin{bmatrix} c_\theta c_\psi & c_\theta s_\psi & -s_\theta \\ s_\phi s_\theta c_\psi - c_\phi s_\psi & s_\phi s_\theta s_\psi + c_\phi c_\psi & s_\phi c_\theta \\ c_\phi s_\theta c_\psi + s_\phi s_\psi & c_\phi s_\theta s_\psi - s_\phi c_\psi & c_\phi c_\theta \end{bmatrix} \end{aligned} \tag{2}$$

An additional reference frame is defined at the hub of each rotor, with its $z$-axis aligned with the axis of rotation. The transformation between the body frame and the hub frame is achieved using a unit quaternion defined by a unit vector about which rotation occurs and the magnitude of that rotation. For torsional cant, the unit vector $\vec{x}_\chi$ (defined in the body-reference frame) and quaternion $q_\chi$ are defined by Eq. 3, and by Eq. 4 for flapwise cant. The rotation matrix is then defined by Eq. 5, where $q_r$, $q_i$, $q_j$, $q_k$ represent the first through fourth entries of either $q_\chi$ or $q_\gamma$. Finally, the rotations are compounded (flapwise, then torsion-wise), resulting in a rotation matrix from the body frame to the hub frame.

$$\begin{aligned} \vec{x}_\chi &= \begin{bmatrix} -\cos\Psi_i & \sin\Psi_i & 0 \end{bmatrix}^T \\ q_\chi &= \begin{bmatrix} \cos\dfrac{\chi}{2} \\ \left(\sin\dfrac{\chi}{2}\right)\vec{x}_\chi \end{bmatrix} \end{aligned} \tag{3}$$

$$\begin{aligned} \vec{x}_\gamma &= \begin{bmatrix} -\sin\Psi_i & -\cos\Psi_i & 0 \end{bmatrix}^T \\ q_\gamma &= \begin{bmatrix} \cos\dfrac{\gamma}{2} \\ \left(\sin\dfrac{\gamma}{2}\right)\vec{x}_\gamma \end{bmatrix} \end{aligned} \tag{4}$$

$$R_{\chi,\gamma} = \begin{bmatrix} 1-2(q_j^2+q_k^2) & 2(q_iq_j-q_kq_r) & 2(q_iq_k+q_jq_r) \\ 2(q_iq_j+q_kq_r) & 1-2(q_i^2+q_k^2) & 2(q_jq_k-q_iq_r) \\ 2(q_iq_k-q_jq_r) & 2(q_jq_k+q_iq_r) & 1-2(q_i^2+q_j^2) \end{bmatrix}$$
$$R_{h/b} = R_\chi R_\gamma \tag{5}$$

In order to satisfy the equilibrium equations defined by the sum of forces and moments about the C.G. in a body-attached reference frame, a trim procedure is established, using the four

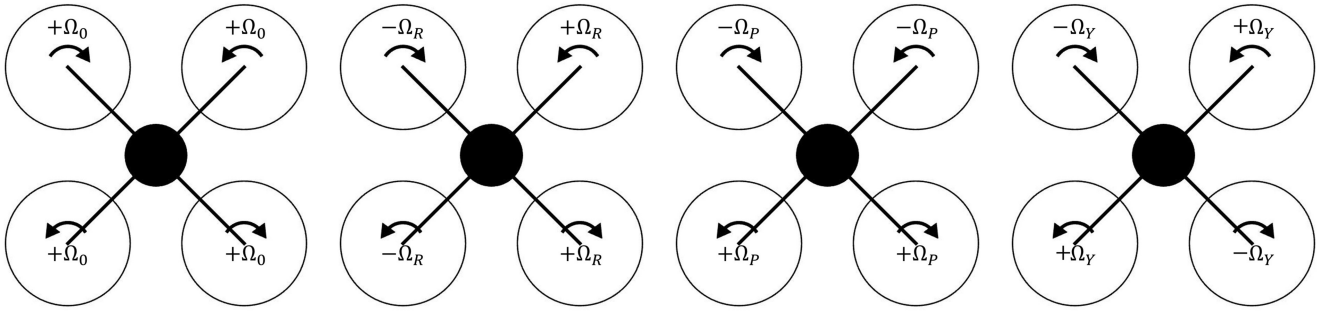


(a) Collective Control ($\Omega_0$) (b) Roll Control ($\Omega_R$) (c) Pitch Control ($\Omega_P$) (d) Yaw Control ($\Omega_Y$)

**Fig. 9. Multirotor controls for a quadcopter**

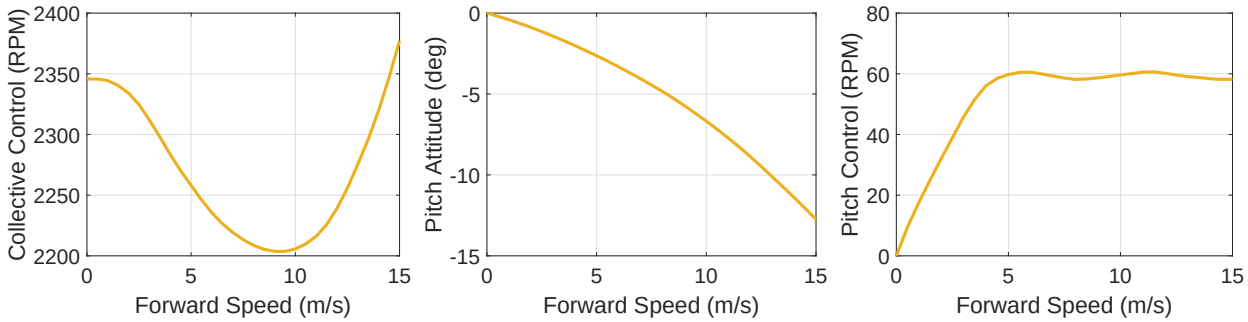


(a) Collective Control (b) Pitch Attitude (c) Pitch Control

**Fig. 10. Trim Controls for baseline quadcopter**

rotor speeds (defined using multi-rotor coordinates), and the roll and pitch attitudes of the aircraft. Solutions are found using the Newton-Raphson method, with the Jacobian numerically estimated. The (time-averaged) rotor inflow states are solved simultaneously with the trim states.

In order to estimate the flight dynamics of the quadcopter, the model is numerically linearized from an equilibrium condition, resulting in a model of the form of Eq. 6. The state vector $x \in \mathbb{R}^{52}$ contains the position (3), attitude (3), velocity (3), angular rates (3), and inflow states ($4\times10$=40). The control vector $u \in \mathbb{R}^4$ contains the control inputs. $A \in \mathbb{R}^{52\times52}$ is the linearized plant model, containing the stability derivatives, and $B \in \mathbb{R}^{52\times4}$ contains control sensitivities. Because the inflow dynamics occur on a much smaller time scale (associated poles far in the left-half plane), the technique of static condensation can be used to reduce the size of the system to $12\times12$. This reduction does not affect the poles associated with rigid body motion, as shown in (Ref. 10).

$$\dot{x} = Ax + Bu \tag{6}$$

## TRIM RESULTS

The required trim controls for a cross-type quadcopter without any rotor cant is presented in Fig. 10. In hover, only thrust needs to be generated, so all four rotors spin at the same speed. At low-speeds, the collective control (Fig. 10(a)) reduces slightly, reflecting the increased efficiency of the rotors at moderate speed, reaching a minimum at 9 m/s. Due to increasing thrust requirements at speeds beyond this, the required collective RPM increases. In order to overcome drag in forward flight, the aircraft needs to pitch nose-down in order to vector its thrust forward, becoming increasingly negative as speed increases (Fig. 10(b)). In order to maintain this nose-down attitude and overcome the hub pitching moment on each rotor (detailed in (Ref. 9)), the rear rotors need to generate more thrust, i.e. spin faster, which is reflected in Fig. 10(c). At the rotor level, the magnitude of the side force, rolling moment, and torque are dependent primarily on the rotor speed, while the direction is dictated by the spin direction of the rotor (e.g. a counter-clockwise-spinning rotor produces a roll-left moment while a clockwise-spinning rotor produces a roll-right moment). By the definition of the multirotor controls in Fig. 9, when using only collective and pitch controls, the two front rotors (and the two rear rotors) spin at the same speed, in opposite directions. Therefore, at the aircraft level, the lateral forces and moments cancel out.

The aerodynamic power (ignoring all inefficiencies associated with the motor and other electronics, as well as interactional aerodynamic effects) required by the quadcopter is shown in Fig. 11. Beginning from a local maximum in hover, the power required to fly reduces in forward flight, as the extra mass

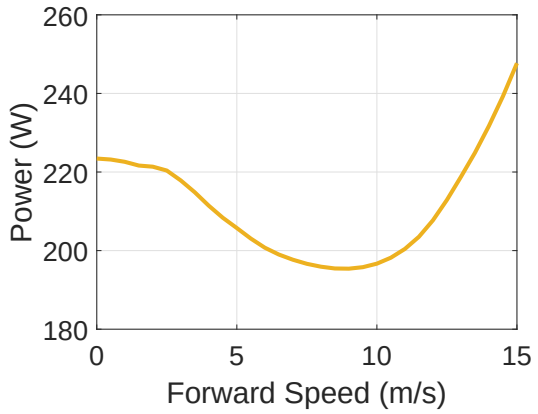


**Fig. 11. Power Required by the quadcopter with no cant**

flux through the disk in edgewise flight reduces rotor-induced velocities. The power reaches a minimum at 9 m/s, and increases beyond that. It is no coincidence that the minimum power occurs at the same speed as the minimum collective control. Aerodynamic power is dominated by the generation of the thrust required to remain aloft, while power associated with generation of moments is relatively small.

### Collective Flapwise Cant ($\gamma_0$)

The required collective RPM to trim for various values of collective flapwise cant is plotted in Fig. 12. For either positive or negative $\gamma_0$, a component of thrust acts either toward or away from the aircraft centerbody. In either case, this causes a reduction in the component acting in the vertical direction, resulting in a slight increase in the required collective control to generate the lift required to maintain trim.

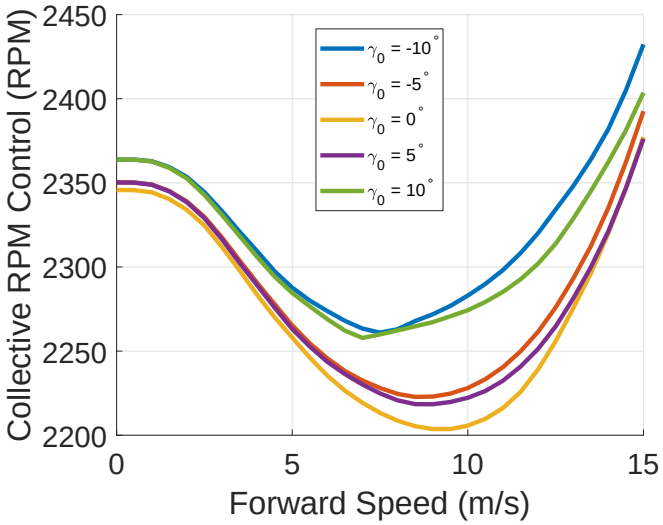


**Fig. 12. Trim controls with different values of collective flapwise cant**

The required pitch control (Fig. 13) changes substantially with $\gamma_0$. As the flapwise cant becomes more positive, the required pitch control increases. For negative values of $\gamma_0$, the required pitch RPM decreases, and even becomes negative above certain speeds (12 m/s for $\gamma_0 = -5°$ and 9.5 m/s for $\gamma_0 = -10°$, indicating that the front rotors are spinning faster than the rear rotors. However, the net nose-up pitch moment at the hub of each rotor is still present and is not affected to the same degree as pitch control (shown for the northeast rotor in Fig. 14), so the rear rotors still need to produce more thrust to maintain attitude.

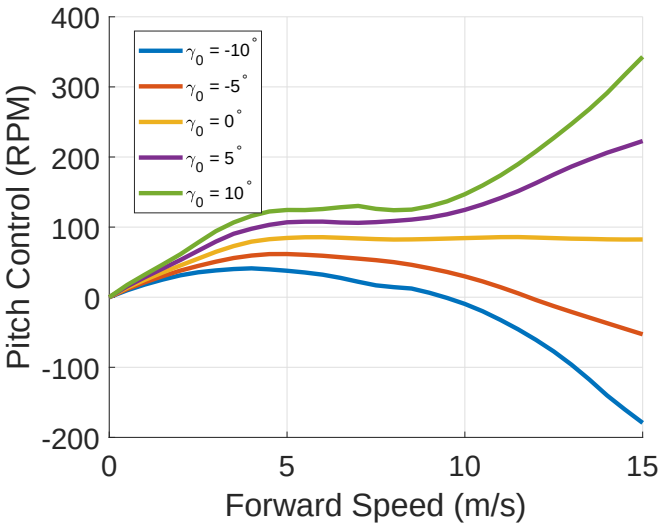


**Fig. 13. Pitch control with different values of $\gamma_0$**

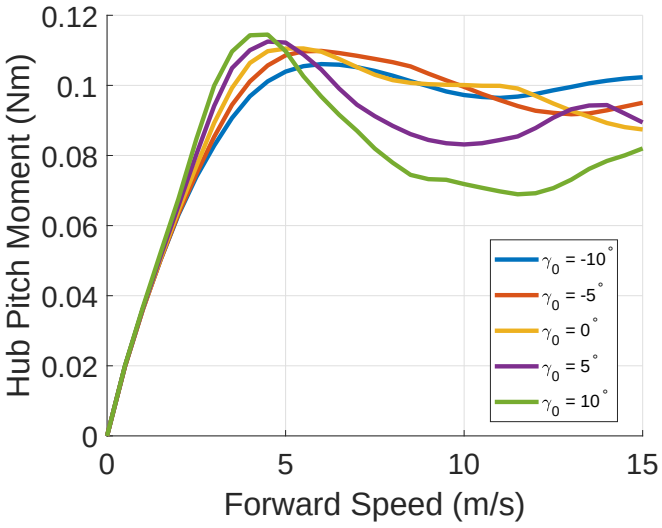


**Fig. 14. Hub pitching moment for the north east rotor at different values of collective flapwise cant**

The rear rotors are canted backwards, so the freestream causes an upwash on the aft rotors, and a downwash on the front rotors (Fig. 15). As a consequence, the rear rotors' thrust increases, while the front rotors' thrust decreases. This phenomenon manifests as a change in the rotor thrust coefficient $\left(T = C_T \rho (\Omega R)^2 (\pi R^2)\right)$, which is plotted versus $\gamma_0$ at 15 m/s forward speed in Fig. 16. The front rotor has a lower $C_T$ for negative values of $\gamma_0$, meaning that they are less efficient in

producing thrust, and that although they are spinning faster, they are producing less thrust than the rear rotors. The other trim controls are not significantly affected.

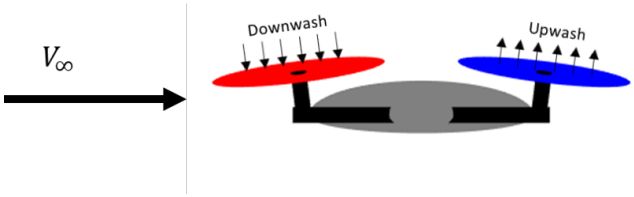


**Fig. 15. Forward speed causes downwash on the front rotors, and upwash on the rear rotors (drawn at zero pitch attitude for clarity)**

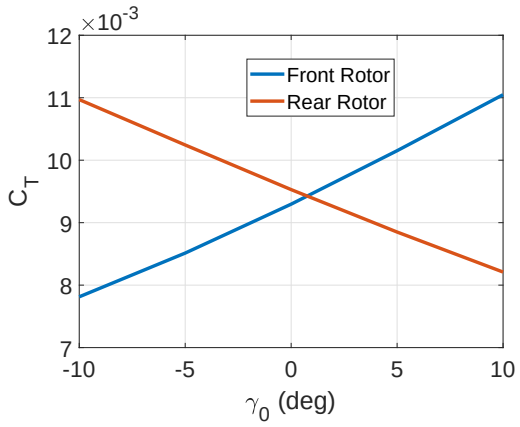


**Fig. 16. Front and rear rotor thrust coefficient for the quadcopter with flapwise cant at 15 m/s**

The power required by the quadcopter is dominated by the mean thrust generated, and thus, collective control. Relative to the uncanted case, $\pm 5^\circ$ and $\pm 10^\circ$ of $\gamma_0$ costs 0.5% and 2.1% in hover power, shown in Fig. 17, but the extra power required increases with forward speed, up to 3.5-4% for $\gamma_0 = \pm 5^\circ$ or 11% for $\gamma_0 = \pm 10^\circ$ at 10.5 m/s. The decrease in relative power at high speed is mostly due to the sharp increase in power required at high speeds.

### Longitudinal Flapwise Cant $\gamma_{1c}$

Application of longitudinal flapwise cant (Fig. 4(c)) causes the two front rotors to redirect their thrust forward and outward laterally, and the rear rotors redirect their thrust forward and inward laterally. This causes a net forward vectoring of thrust, which requires a more-nose up (or less nose-down) attitude, relative to the uncanted system (Fig. 18) by $\gamma_{1c}/2$. Figure 19 illustrates the component of rotor hub torque that acts in the body frame XY-plane. The torques balance about the roll axis, but compound about the pitch axis, resulting in a nose-down pitching moment. Combined with the forward reorientation of thrust, acting above the aircraft C.G., this reduces the required pitch control input (Fig. 20)

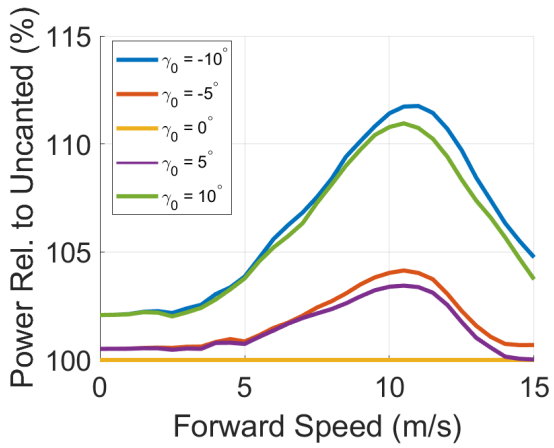


**Fig. 17. Relative power costs for different values of $\gamma_0$**

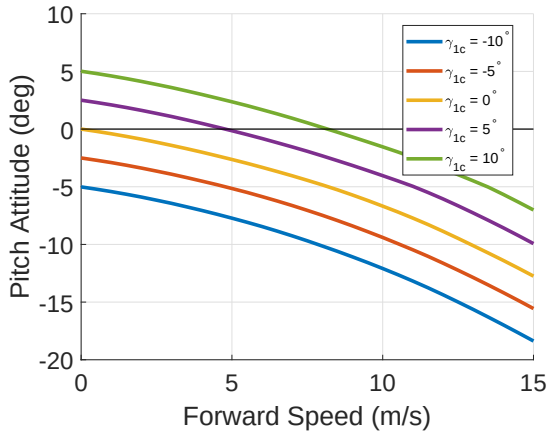


**Fig. 18. Pitch attitude for different values of $\gamma_{1c}$ (Positive nose-up)**

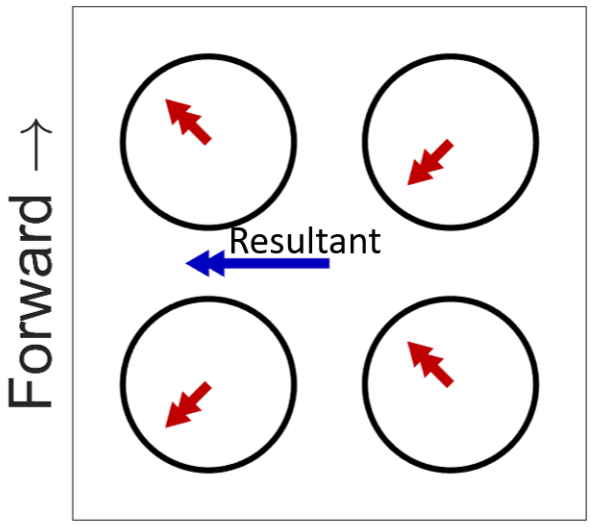


**Fig. 19. Vector representation of in-plane component of hub torque (Resultant in blue)**

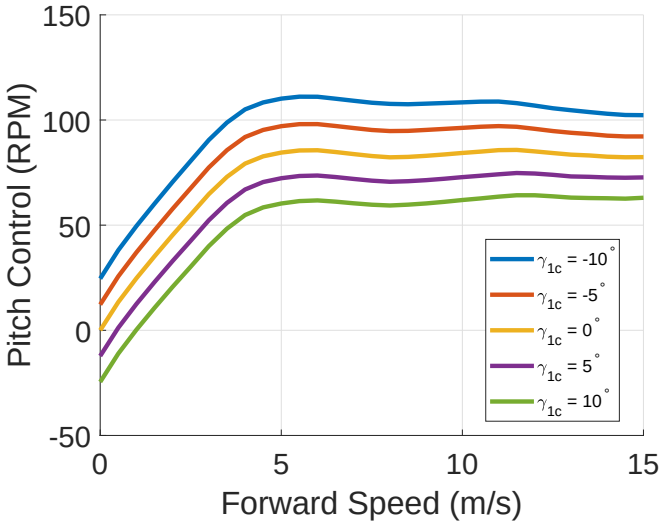


**Fig. 20. Pitch control for different values of $\gamma_{1c}$**

Critically, the reduced pitch attitude changes the forces on the fuselage. At 15 m/s, the reduced pitch attitude associated with 10°of $\gamma_{1c}$ reduces the fuselage drag by 13%, and the (negative) lift by 31% (see Fig. 2). The latter corresponds to a reduction of 1.6N of required thrust generation (5% of the aircraft gross weight). This reduction in thrust required directly results in a reduction in the collective control and power requirement by 6% while increasing hover power by only 0.5% (Fig. 21).

### Lateral Flapwise Cant ($\gamma_{1s}$)

Lateral flapwise cant causes the rotors on the right side of the aircraft to thrust leftward and inward longitudinally, while the rotors on the left thrust leftward and outward longitudinally. Much like $\gamma_{1c}$ resulted in a net forward thrust (and change in pitch attitude), $\gamma_{1s}$ causes a net leftward thrust (compensated for by a change in roll attitude, Fig. 22). The cant also causes a component of the hub torque to act in the aircraft roll direction (see Fig. 23), and the lateral tilt of the rotor thrust (above the aircraft C.G.) produces a roll moment. Unlike the case of pitch moment with $\gamma_{1c}$, these two roll moments act in opposite directions, and, by coincidence, cancel. If the vertical position of the rotors relative to the C.G. changes, these effects will not cancel completely.

The only other trim control that is substantially impacted by $\gamma_{1s}$ is the yaw control input. Consider the northeast rotor with positive $\gamma_{1s}$, located at $\Psi = 135°$, which spins counterclockwise. In forward flight, this rotor produces a substantial roll-left moment due to asymmetry in dynamic pressure. When this rotor tilts rearward, a component of this moment acts in the yaw direction, causing a nose-left moment. The same occurs for the southwest rotor, which also tilts backward and spins counterclockwise. The two clockwise-spinning rotors tilt forward, which causes their roll-right moments to create nose-left yaw moments. Altogether, there is a substantial nose-left moment, which is countered by positive $\Omega_d$ (Fig. 24).

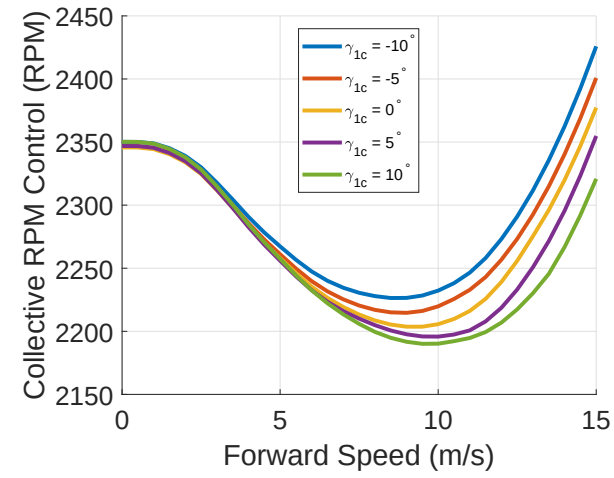


(a) Collective control for multiple values of $\gamma_{1c}$

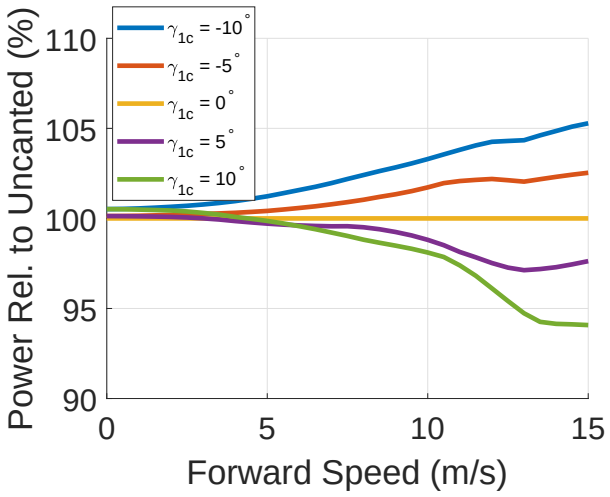


(b) Relative power for multiple values of $\gamma_{1c}$

**Fig. 21. Collective control and power consumption for multiple values of $\gamma_{1c}$**

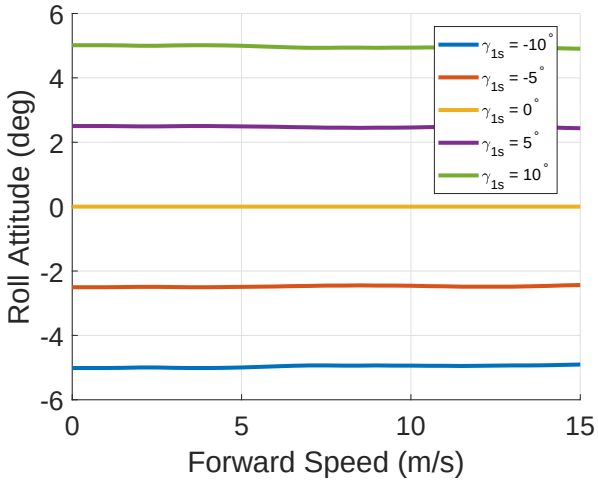


**Fig. 22. Roll attitude for different values of $\gamma_{1s}$ (Positive roll-right)**

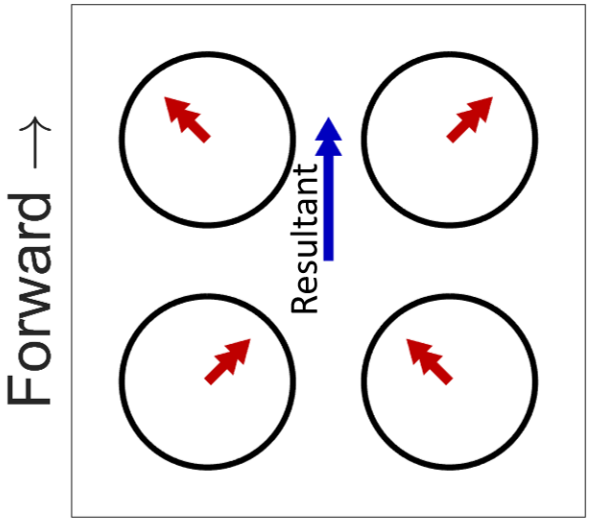


**Fig. 23. Vector representation of in-plane component of hub torque (Resultant in blue)**

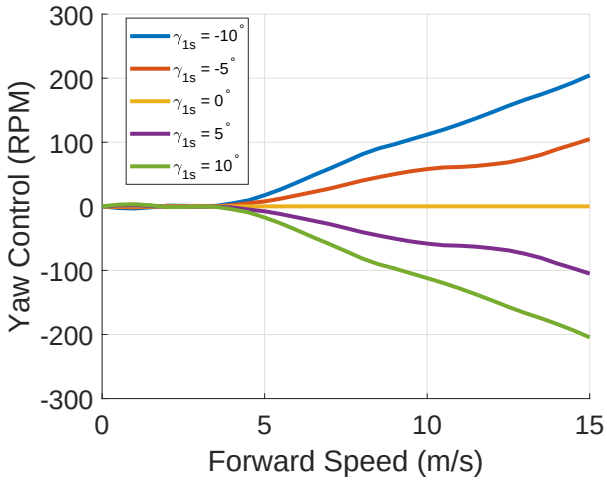


**Fig. 24. Yaw control for different values of $\gamma_{1s}$**

Generally speaking, the power requirement is greater when either positive or negative $\gamma_{1s}$ is applied (Fig. 25). This increase in power requirement is due to the reduction in the component of rotor thrust that acts directly against gravity. In Fig. 25, the curves for $\gamma_{1s} = -5, -10$ lie under the curves for $\gamma_{1s} = +5, +10$, respectively, indicating that only the magnitude of the cant is relevant for power consumption. Overall, the penalty is less than was observed for $\gamma_0$.

### Differential Flapwise Cant ($\gamma_d$)

Differential flapwise cant (Fig. 4(d)) causes the counterclockwise-spinning rotors to redirect thrust away from the fuselage and the clockwise-spinning rotors to redirect thrust toward the fuselage. The most substantial impact this has is on the required roll control (Fig. 26). To explain this, consider the right side of the aircraft as shown in Fig. 4(d). Both of the rotors on this side of the aircraft have

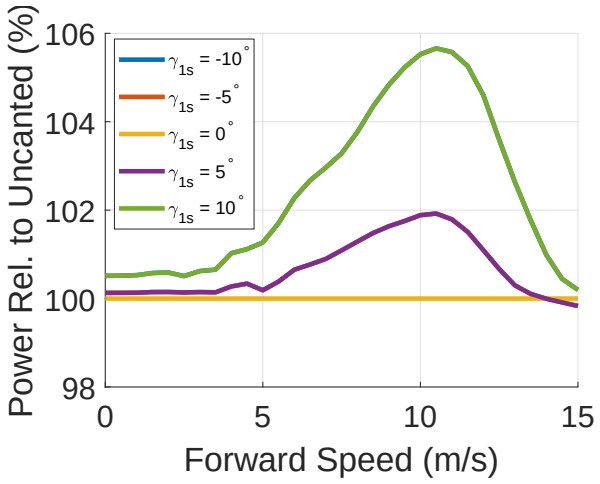


**Fig. 25. Relative power consumption for different values of $\gamma_{1s}$**

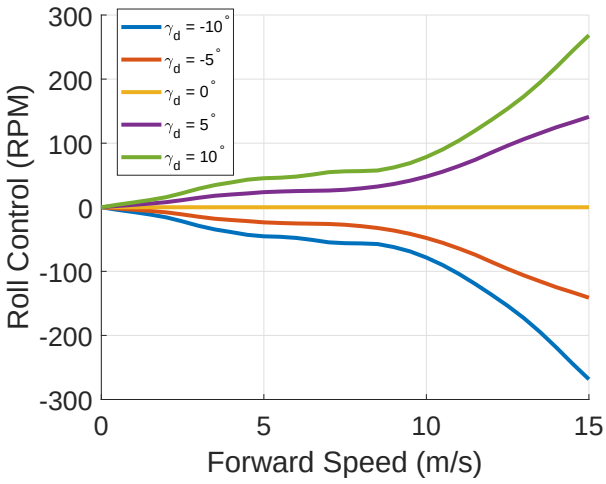


**Fig. 26. Required roll control for different values of $\gamma_d$**

their rotors tilt forward, while the rotors on the left side of the aircraft tilt backward. In forward flight, a component of the freestream acts as downwash on the right side and upwash on the left, which causes a roll-right moment, which must be countered by positive roll control.

As with $\gamma_0$ and $\gamma_{1s}$ the primary influence of $\gamma_d$ on power is the redirection of thrust from the body heave axis. This redirection increases the thrust that must be produced by each rotor, increasing the power consumption (Fig. 27). Again, the curves for negative $\gamma_d$ lie beneath the curves for positive $\gamma_d$, indicating that only the magnitude affects the power consumption in trim.

### Longitudinal Torsional Cant ($\chi_{1c}$)

Application of longitudinal torsional cant (Fig. 6(c)) redirects rotor thrust on the right side of the aircraft leftward and outward longitudinally, and rotor thrust on the left side leftward and inward longitudinally. This makes it very similar to $\gamma_{1s}$, except the longitudinal directivity of each rotor is reversed.

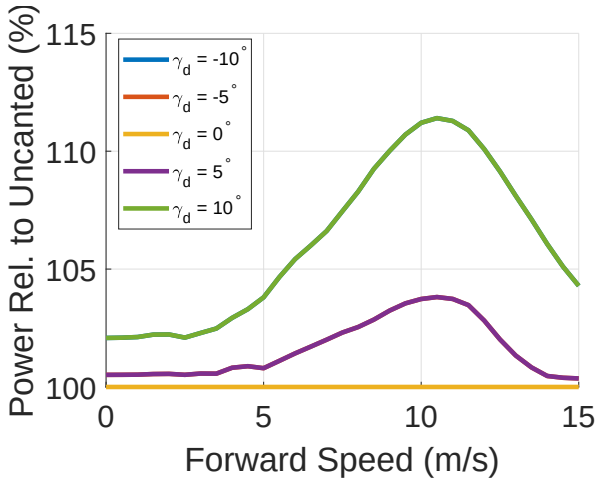


**Fig. 27. Relative power consumption in trim for different values of $\gamma_d$**

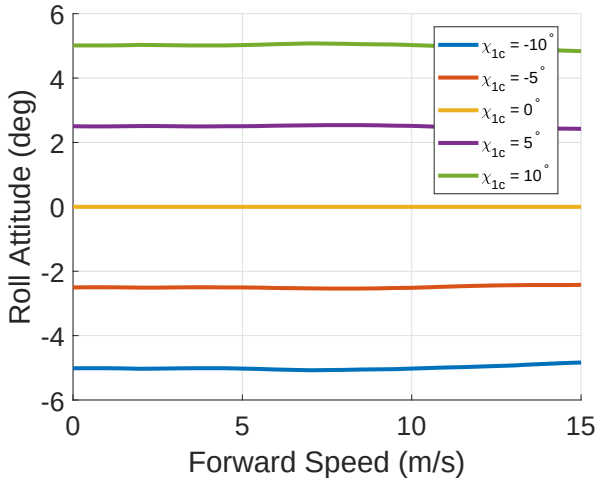


**Fig. 28. Roll attitude for different values of $\chi_{1c}$**

Naturally, this causes trim behavior nearly identical to the lateral flapwise cant, except the sign of the rotor-roll to aircraft-yaw coupling is reversed (compare Figs. 28 and 29 to Figs. 22 and 24). Power consumption is similarly correlated (compare Fig. 30 to Fig. 25).

### Lateral Torsional Cant ($\chi_{1s}$)

Lateral torsional cant is depicted in Fig. 6(b). In this mode, the rear rotor thrusts are redirected rearward and inward laterally, and the front rotors' thrusts are redirected rearward and outward laterally, resulting in a net rearward thrust (so that negative $\chi_{1s}$ is very similar to positive $\gamma_{1c}$). As the $\chi_{1c}$ trim controls were analogous to the $\gamma_{1s}$ trim controls, so too are the $\chi_{1s}$ controls largely analogous to the $\gamma_{1c}$ controls (Compare Figs. 18 and 20 to Figs. 31 and 32). The only major differences are that positive $\chi_{1s}$ corresponds to negative $\gamma_{1c}$ and vice-versa, and that $\chi_{1s}$ introduces only small effects on the pitch control, since the two effects that compounded to change pitch control for $\gamma_{1c}$ (forward thrust above C.G. and the redirection of hub torque) now act in opposite directions for $\chi_{1s}$. As with $\gamma_{1c}$, the reduction in pitch attitude for negative $\chi_{1s}$ reduces the negative lift and the drag on the fuselage, reducing collective RPM and power consumption (Fig. 33).

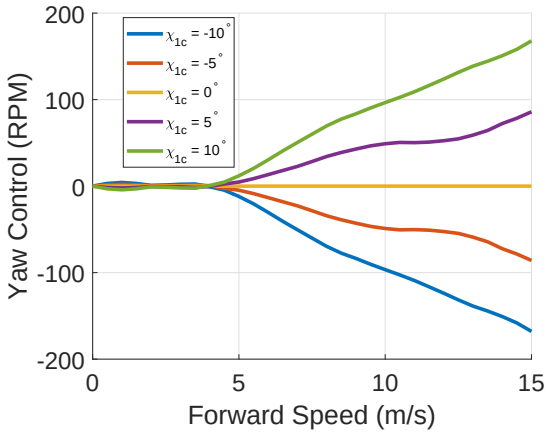


**Fig. 29. Yaw control for different values of $\chi_{1c}$**

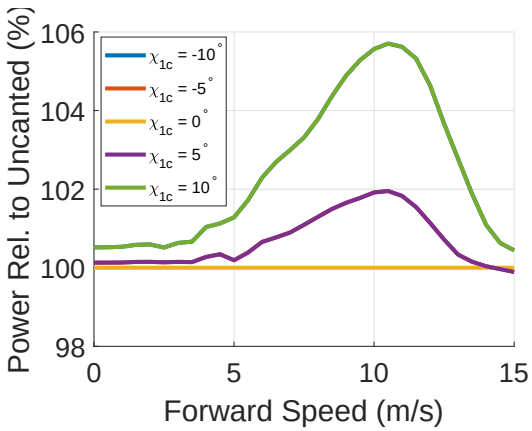


**Fig. 30. Relative power requirement for different values of $\chi_{1c}$**

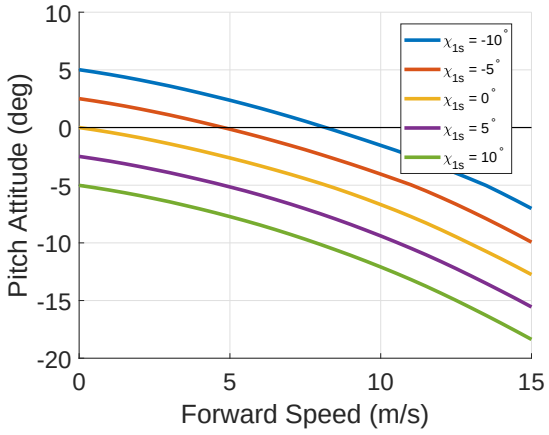


**Fig. 31. Pitch attitude for different values of $\chi_{1s}$**

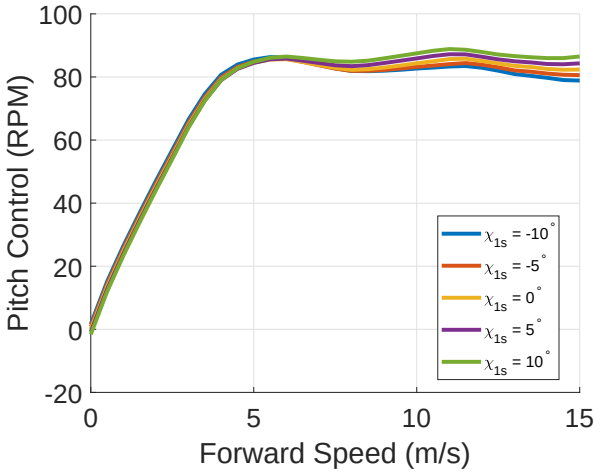


**Fig. 32. Pitch controls for different values of $\chi_{1s}$**

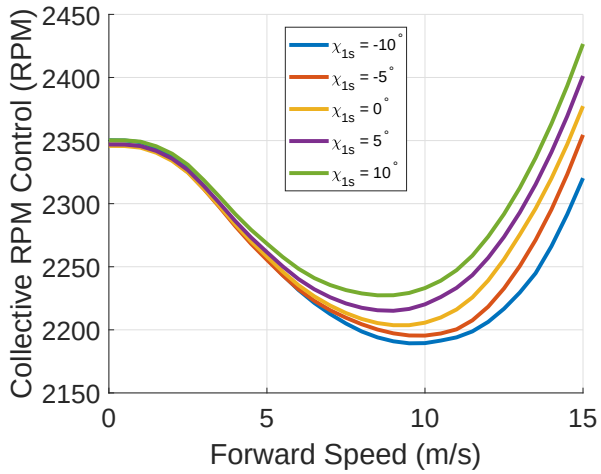


(a) Collective control

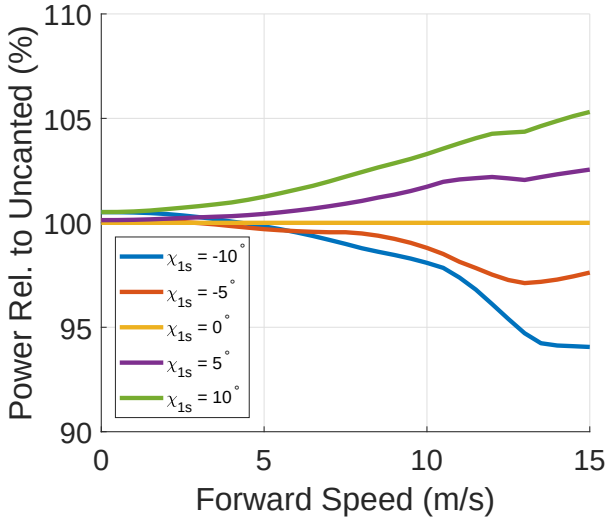


(b) Relative power

**Fig. 33. Collective control and power consumption for multiple values of $\chi_{1s}$**

**Differential Torsional Cant ($\chi_d$)**

Differential torsional cant (Fig. 6(d)) directs the thrust from the front two rotors forward and inward laterally, and the rear two rotors rearward and inward laterally. If positive $\chi_d$ is applied, a component of the freestream velocity acts as upwash on the rear rotors and downwash on the front rotors, which causes a nose-down moment, reducing the required pitch control, similar to $\gamma_0$ (Compare Figs. 13 and 34). Aside from that, the collective control and power consumption are identical to the $\gamma_0$ case (except positive $\chi_d$ corresponds to negative $\gamma_0$).

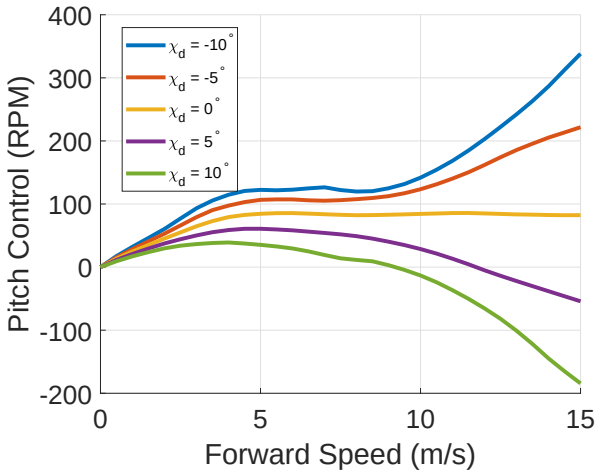


**Fig. 34. Pitch control for different values of $\chi_d$**

## LINEAR DYNAMICS

After numerically linearizing the quadcopter model about an equilibrium condition, the flight dynamics are described by Eq. 6. As the reduced system is a 12-state model, there are twelve open-loop poles associated with the eigenvalues of $A$, plotted for the aircraft with zero cant in hover in Fig. 35. The eigenvectors associated with these eigenvalues represent the dynamic modes of the quadcopter. There are four poles located at the origin, corresponding to the position states and the heading. There are two poles located at $\lambda = -2.342$ corresponding to the pitch and roll subsidence modes, one pole at $\lambda = -0.4834$ corresponding to the heave mode, one pole at $\lambda = -0.114$ corresponding to the yaw rate mode, and two pairs of complex conjugate poles at $\lambda = 0.7026 \pm 1.689i$ corresponding to the longitudinal and lateral phugoid modes. These poles are also tabulated in Table 1. Only collective and differential flapwise cant, and differential torsional cant, have any significant impact on the locations of these poles in hover.

**Table 1. Dynamic Poles for uncanted quadcopter in hover**

| Pole | Mode | Pole | Mode | Pole | Mode |
|---|---|---|---|---|---|
| 0 | $x$-position | -0.114 | Yaw Rate | $0.7026 \pm 1.689i$ | Longitudinal Phugoid |
| 0 | $y$-position | -0.4834 | Heave | | |
| 0 | $z$-position | -2.342 | Pitch Subsidence | $0.7026 \pm 1.689i$ | Lateral Phugoid |
| 0 | Heading | -2.342 | Roll Subsidence | | |

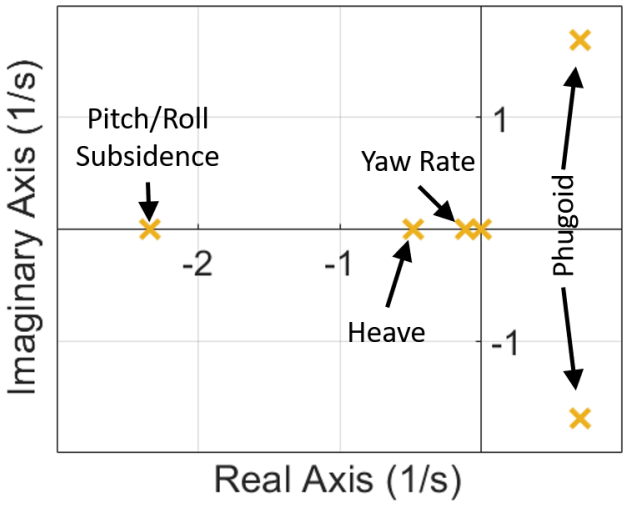


**Fig. 35. Open loop poles for the baseline aircraft**

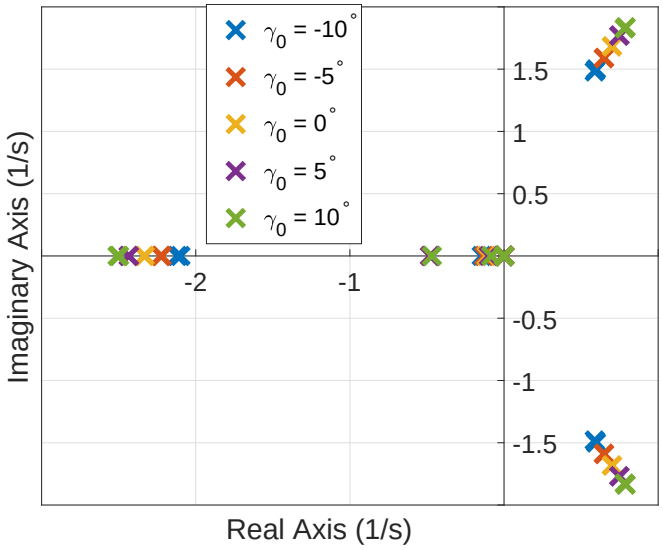


**Fig. 36. Open loop poles in hover for different values of $\gamma_0$**

### Collective Flapwise Cant

The location of the poles in hover for different values of $\gamma_0$ is plotted in Fig. 36. The largest effect $\gamma_0$ has is on the longitudinal and lateral dynamics. As $\gamma_0$ becomes more positive, both the phugoid modes and the subsidence modes move away from the origin, with the former becoming less stable and the latter becoming more stable. The cause of the pole motion is the change in the stability derivative $M_u$, that is, the sensitivity of pitch acceleration to longitudinal velocity. As $M_u$ becomes more positive, the real and imaginary components of the phugoid mode poles tend to grow in magnitude, as does the subsidence mode poles. The only other substantial contributor to these poles is $M_q$, that is, the sensitivity of pitch acceleration to pitch rate, or pitch damping, which tends to make all of these poles more stable. Both stability derivatives are plotted in Fig. 37, and it can be seen that $M_u$ is positively correlated with $\gamma_0$, and $M_q$ is unaffected. Because the axisymmetry of the aircraft is preserved by $\gamma_0$, the lateral dynamics are affected in the same way by $\gamma_0$, and the poles coincide.

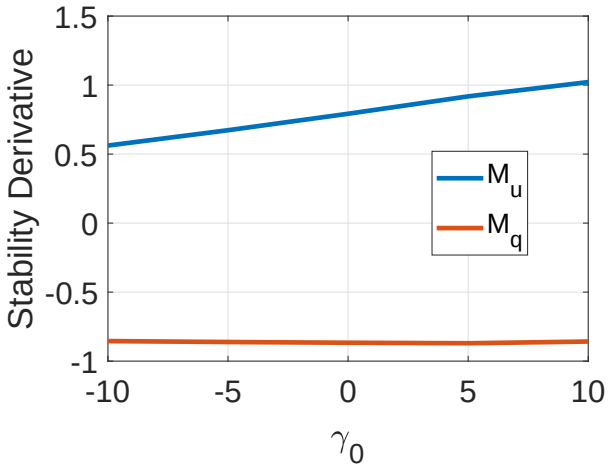


**Fig. 37. Longitudinal dynamics stability derivatives in hover versus $\gamma_0$**

### Differential Flapwise Cant

When $\gamma_d$ is applied, the axisymmetry of the aircraft is broken, and longitudinal and lateral dynamics are no longer identical. In fact, the phugoid and subsidence modes are reoriented to align with the booms of the aircraft, so that one phugoid mode oscillates north-east to south-west (NE-SW, see Fig. 8), and the other oscillates south-east to north-west (SE-NW). For positive $\gamma_d$ (Fig. 4(d)), the NE-SW mode behaves as though negative $\gamma_0$ were applied (rotors along this axis thrust away from the centerbody, compare Figs. 5(a) and 5(d)) , and the SE-NW mode acts as though positive $\gamma_0$ were applied, and vice-versa for negative $\gamma_d$ (compare Figs. 5(a) and 5(d)). Thus, as $\gamma_d$ changes, one set of three poles moves (associated with NE-SW motion) toward the origin, while the other set

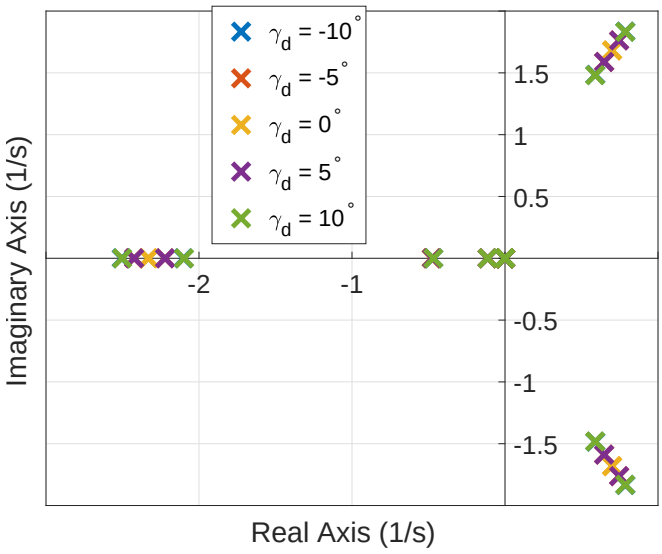


**Fig. 38. Open loop poles in hover for different values of $\gamma_d$**

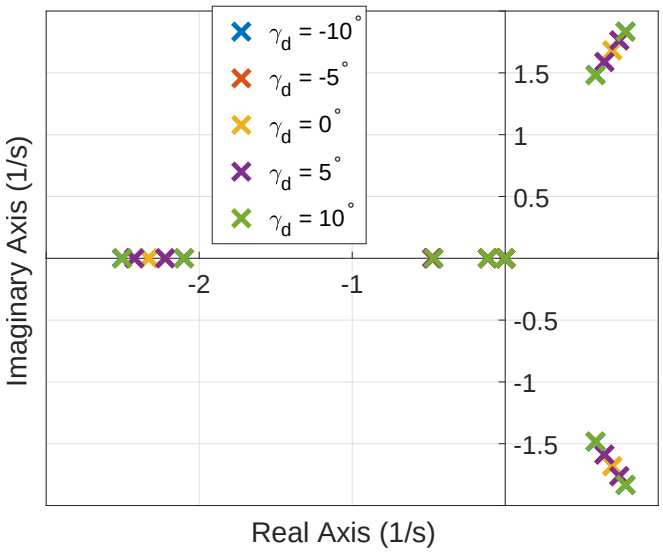


**Fig. 39. Open loop poles in hover for different values of $\chi_d$**

of three poles (associated with SE-NW motion) moves away (Fig. 38).

### Differential Torsional Cant

As when $\gamma_d$ was applied, the axisymmetry of the aircraft is broken when $\chi_d$ is applied, so longitudinal and lateral dynamics are no longer identical. However, $\chi_d$ tends to align the phugoid modes between the booms of the quadcopter, which happen to align with the flight axes. The open loop poles are plotted in Fig. 39. For positive $\chi_d$, the upwash on the rear rotors and downwash on the front rotors in forward flight reduces $M_u$, causing the longitudinal poles to move toward the origin. Considering the lateral axis, a rightward aircraft velocity causes upwash through the right rotors, and downwash through the left, causing a roll-left moment, enhancing the sensitivity of roll acceleration to lateral velocity, causing the lateral poles to move away from the origin. Negative $\chi_d$ does the opposite, making the longitudinal phugoid mode less stable, and the lateral phugoid mode more stable.

Unique among the eight cant modes defined in Figs. 4 and 6, $\chi_d$ also has a significant effect on the control sensitivity matrix, $B$, in Eq. 6, specifically on the relationship between $\Omega_d$ (Fig. 9(d)) and yaw acceleration. In the absence of cant, increasing the speed of the counter-clockwise-spinning rotors while reducing the speed of the clockwise-spinning rotors produces a net nose-right reaction torque on the aircraft. When positive $\chi_d$ is applied, a component of rotor thrust also serves to produce a yaw moment, with the counter-clockwise rotor thrust producing a nose-left moment, and the clockwise rotor thrust produces a nose-right moment. When $\Omega_d$ is applied, the counter-clockwise-rotor thrust is increased, and the clockwise-rotor thrust is decreased, producing a net nose-left moment, opposite that induced by the hub reaction torque. For negative $\chi_d$, these two effects act in the same direction. The sensitivity of yaw acceleration to $\Omega_d$ is plotted in Fig. 40. With $\chi_d = -10°$, the sensitivity of yaw acceleration to $\Omega_d$ is

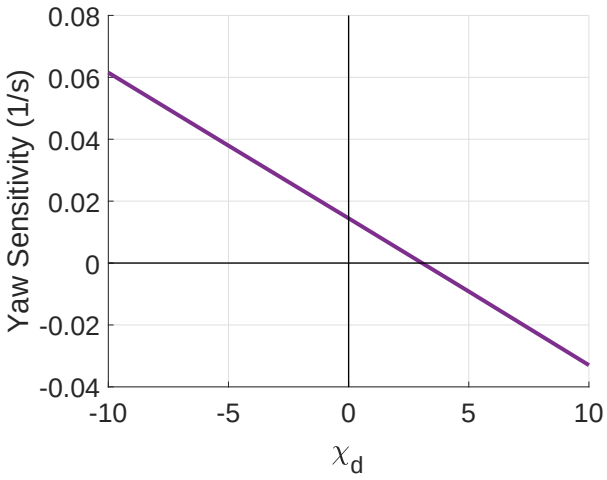


**Fig. 40. Yaw acceleration-$\Omega_d$ in hover sensitivity for different values of $\chi_d$**

increased by 325%, for a maximum of 12% increase in power. A 162% increase in sensitivity can be obtained with $\chi_d = -5°$ for a maximum of 4.2% increase in power.

## CONCLUSIONS

An SUI Endurance was modified by applying various types of cant to its rotors. Four aircraft-level modes were defined for cant for two different types of rotor cant, and their effects on predicted trim controls and linear flight dynamics estimated.

Application of collective flapwise cant resulted in a general increase in required collective RPM control, and a positive correlation between $\gamma_0$ and pitch control was found. This was due to the freestream acting as downwash or upwash, depending on the orientation of the rotor. Power was increased by 0.5% ($\gamma_0 = \pm 5°$ in hover) to 11% ($\gamma_0 = \pm 10°$ at 10.5 m/s). Similar effects were found for $\chi_d$, except with a negative correlation between $\chi_d$ and pitch control. Longitudinal flapwise

cant and lateral torsional cant both result in rotors canting forward, and so they have similar effects, most importantly, a positive (negative) correlation between $\gamma_{1c}$ ($\chi_{1s}$) and pitch attitude. In general, if $k^\circ$ of $\gamma_{1c}$ (or $-k^\circ$ of $\chi_{1s}$) is applied, the pitch attitude in trim increases (becomes more nose-up) by $k/2^\circ$. When the pitch attitude, negative in forward flight, is reduced (so that the aircraft flies more nose-level), the negative lift and the drag of the fuselage is similarly reduced, by 31% and 13% at 15 m/s for $\gamma_{1c} = 10^\circ$ (or $\chi_{1s} = -10^\circ$), reducing overall aircraft power at 15 m/s by 6%, with only a 0.5% increase in hover power. Lateral flapwise cant (and longitudinal torsional cant) have similar effects on the lateral direction, though no power savings is available through changing the roll attitude. Additionally, because a component of the hub roll moment applies in the yaw direction, a negative correlation between $\gamma_{1s}$ and yaw control is found. Similarly, $\chi_{1c}$ affects yaw control, but in the opposite direction. Finally, $\gamma_d$ caused a change in the roll control in trim, due to a relative downwash on right-side rotors, and an upwash on left-side rotors.

Application of positive collective flapwise cant causes the poles associated with the longitudinal and lateral dynamics to move away from the origin. This pole motion is caused by a change in the sensitivity of pitch acceleration to forward speed, caused by the same relative upwash/downwash that changes the pitch control. Differential flapwise cant breaks the symmetry of the aircraft, so the longitudinal and lateral poles are no longer coincident. Additionally, the phugoid and subsidence modes become oriented along the booms, rather than on the flight axes. For positive or negative $\gamma_d$, one set of modes moves away from the origin, while the other set moves toward the origin. $\chi_d$ also breaks the symmetry of the aircraft, and the longitudinal/lateral modes are oriented between the booms (due to the layout of the rotors, they coincide with the flight axes). Positive $\chi_d$ causes the longitudinal modes to move toward from the origin, making the phugoid modes less unstable. $-10^\circ$ ($-5^\circ$) of $\chi_d$ causes a 325% (162%) increase in the yaw authority of the quadcopter, by redirecting the thrust of all four rotors so that the rotor thrust differential caused by yaw control adds to the hub counter-torque, at a maximum of 12% (4.2%) increase in power.

## ACKNOWLEDGMENTS

The authors acknowledge the Department of Defense and the American Society for Engineering Education for supporting Robert Niemiec through the National Defense Science and Engineering Graudate (NDSEG) Fellowship.

## REFERENCES

[1]Giannini, F., Kaufman, A., and Kearney, M., "Configuration Development and Subscale Flight Testing of an Urban Mobility eVTOL," Proceedings of the AHS International Technical Meeting on Aeromechanics Design for Transformative Vertical Lift, San Francisco, CA, Jan. 16-18, 2018, 2018.

[2]Hilbert, K., "A Mathematical Model of the UH-60 Helicopter," Technical Memorandum 85890, NASA, 1984.

[3]Brescanini, D. and D'Andrea, R., "Design, Modeling, and Control of an Omni-Directional Aerial Vehicle," Proceedings of the 2016 International Conference on Robotics and Automation, Stockholm, Sweden, 2016.

[4]Phillips, B., Hrisikeshavan, V., Yeo, D., and Chopra, I., "Experimental Evaluation of a Quadrotor Biplane with Variable Pitch Rotors," 73rd Annual Forum of the American Helicopter Society, Fort Worth, Texas, 2017.

[5]"Products — STRAIGHT UP IMAGING," http://www.straightupimaging.com/products/.

[6]Russell, C. and Sekula, M., "Comprehensive Analysis Modeling of Small-Scale UAS Rotors," 73rd Annual Forum of the American Helicopter Society International, Fort Worth, Texas, 2017.

[7]Russell, C., Jung, J., Willink, G., and Glasner, B., "Wind Tunnel and Hover Performance Test Results for Multicopter UAS Vehicles," 72nd Annual Forum of the American Helicopter Society International, West Palm Beach, Florida, 2016.

[8]Niemiec, R. and Gandhi, F., "Multi-rotor Coordinate Transforms for Orthogonal Primary and Redundant Control Modes for Regular Hexacopters and Octocopters," 42nd European Rotorcraft Forum, Lille, France, 2016.

[9]Niemiec, R. and Gandhi, F., "Effect on Inflow Model on Simulated Aeromechanics of a Quadrotor Helicopter," 72nd Annual Forum of the American Helicopter Society International, West Palm Beach, Florida, 2016.

[10]Niemiec, R. and Gandhi, F., "Multirotor Controls, Trim, and Autonomous Flight Dynamics of Plus- and Cross-Quadcopters," *Journal of Aircraft*, 2017.